Chapter IV

CHAPTER IV

CHARACTERIZATION TECHNIQUES

4.1 Introduction

The fundamental techniques used for the characterization of nanomaterials were discussed in this section. The physical characteristics of prepared nanoparticles are studied by X-Ray Diffraction technique. The morphology examined using Transmission Electron Microscopy, Scanning Electron Microscopy, Energy Dispersive X-ray Analysis & Fourier Transform Infrared Spectroscopy. UV-Visible Spectroscopy were utilized to examine the optical properties.

4.2 X - Ray Diffraction Technique (XRD)

The area of diffracting X-rays using crystals was firstly viewed in 1912. When the substance was determined, X-ray crystallography can be utilized to describe their structure. By considering the interatomic distance & angle the arrangement of atom in crystalline phase can be known. XRD is a significant technique utilized by solid state chemistry & material science. XRD technique used to characterize packing of atoms inside the crystal and their distance between the crystal phases [1].

4.2.1 Experimental set up for XRD

X-Ray Diffraction technique was used to determine the crystalline nature & the size for synthesized nanoparticles. Characterization of Co_3O_4 nanoparticles were done by utilizing SHIMADZU Lab XRD 6000 using CuKα radiation monochromatic filter between10-80^o. Using Debye-Scherer equation, particle size for the Cobalt oxide nanoparticles was calculated.

The constructive interference between monochromatic X-rays & material with crystallinity is the root of X-Ray Diffraction technique that fulfills the Bragg's Law [2]:

$$n\lambda = 2d\sin\theta \qquad (4.1)$$

Whenever, X-rays incident on crystal surfaces, 'θ' angle of incidence would reflect by similar angle of scattering 'θ'. While,'d' difference in path equals to an integer 'n', wavelength 'λ' then constructive interference would happen. X- ray beams intersect

with electron group were spaced at regular distance. Intensity of scattered X-rays is in accordance to the number of electrons that the X-ray is scattered from.

Scherrer's formula correlates size of particles inside the crystals in powder form. It is applicable only to nanoparticles. Scherrer equation is limited to grains greater than about 0.2 μm [3]. Scherrer's formula is expressed as:

$$D = 0.89 \lambda / (\beta \cos\theta) \quad (4.2)$$

Here, crystallite size (D) in nm, wavelength of incident X-ray (λ) is1.5406 m, full width at half maximum (β) & diffraction angle (θ). Generally, the value of K is 0.89 because the range of shape factor (K) is between 0.62 - 2.08.

4.2.2. Working Principle

X-ray tube, sample holder & X-ray detector are the main parts of X-ray diffractometers. The image of an XRD instrument is shown in figure 4.1

X-rays were produced inside cathode ray tube through heating the filament to create electrons, encouraging electrons to the target through providing voltage & attacking target substance by electrons. Whenever electrons attain adequate energy to displace inner shell electrons of target substance, X-ray spectra were formed. The spectra contain various components, commonly K_α & K_β. K_α includes $K_{\alpha1}$ & $K_{\alpha2}$. $K_{\alpha1}$ had lightly shorter wavelength & double intensity as $K_{\alpha2}$. These particular wavelengths were properties of target material (Cr, Fe, Cu, Mo).

Filtrating through foils was needed to create monochromatic X-ray required for diffraction. $K_{\alpha1}$ & $K_{\alpha2}$ were adequately similar in wavelength like a moderate weight of both is utilized. For single crystal diffraction, the commonly used target material is copper having Cu K_α radiation = 1.5418 Å that were collimated & pointed to sample.

The X-ray diffractometer is figured by the sample circulates in way of collimated X-ray at an angle 'θ'. X-ray detector is established on an arm to acquire diffracted X-rays & revolves at 2θ angle. A goniometer is utilized to regulate angle & circulate sample. X-rays pointed to a sample attached on goniometer were diffracted through the sample.

The peaks of diffracted X-rays were constantly recorded during sample & detector circulates with respective angles were plotted. The output is termed as the X-ray diffraction graph of material. A detector reports & executes X-ray signals & changes to a count rate that is connected to a printer/monitor. Computer evaluation of peaks & intensities related to the graph that permits qualitative analysis, determining lattice constants & stress of sample. Qualitative evaluation can also be performed on the foundation of peak intensity. The datas are utilized to decide particle diameters, crystallinity & for specific X-ray structural evaluation [4].

Figure: 4.1 XRD Instrument

4.3. Transmission Electron Microscopy (TEM)

The technique utilized for observing the properties of tiny particles in a magnified pattern upto 2 million times are termed as Transmission electron microscopy. Using TEM, specimens are viewed at atomic level, which is less than 1nm. These features are utilized in medical investigations such as forensic science, materials science & geomology.

The electron microscopes were discovered by Louis de Broglie in1920 through the development of cathode rays. Then lenses for electrons are utilized by magnetic fields finally, first electron microscope was established by Ernst Ruska & Max Knolls in 1931. After 2 years, it is developed to a Transmission Electron Microscope through Siemen's company.

The TEM microscope had many merits than light microscope because of its high efficiency. The particle of 2 nm can be magnified with a resolution limit of 0.2 μm. It can provide information about morphology, structure, crystallization & stress of specimen. The high resolution is obtained due to the shorter wavelength of electron than a photon. Anyway, TEM needs thinner samples, partially transparent to electrons that take much time for preparing specimen [5].

4.3.1. Experimentation of a Transmission Electron Microscope (TEM)

The electron gun having heated tungsten filament creates electrons which are focused using condenser lenses on to the sample. Through aid of column tube of condenser lens to vacuum producing a clear image, electrons create a clear image without bombardment by any air molecules. When it hits the sample, it scattered the electrons targeting them on magnetic lenses producing a clear large image. When it passes via fluorescent screen, polychromatic image is formed. A dark image is formed from denser sample for scattering more electrons due to lesser electron attains the screen for visualization. Meanwhile thinner, much transparent samples are brighter. When screen is kept aside, a photograph in pixels creating a static photograph is obtained.

4.3.2. Parts of Transmission Electron Microscope (TEM)

Electron gun, Image producing system and Image recording system are the three main parts of TEM.

Electron beams are produced by electron gun in the TEM. The V-shaped tungsten filament which heated normally that lies upper or lower of the cylindrical holes act as a cathode provides electrons. Wehnelt cylinder, the control grid that covers the cathode with hole in the centre lie column like tube. Tungsten filament & Wehnelt cylinder were negatively charged. At high voltage, the electrons from cathode were transferred to anode through a column like hole by a static energy for creating précised image by pointing the sample efficiently. By maintaining column aperture of electron gun and energy, condenser lens apparatus performs to target electron beam on sample. The TEM utilizes both condenser lenses to combine beam of electrons to sample. The small image of sample having stronger magnification was produced by first lens & second condenser lens points the photograph to objectives.

Image- Producing system consists of objective lens, moving stage to hold the sample, and intermediate & projector lenses. An extremely enlarged imaged is obtained by targeting the electrons travelling through the sample. The focal length of an objective lens is shorter i.e, 1-5mm. The intermediate image for magnification was transmitted from the condenser to projector lenses. The 2 types of projector lenses are intermediate lens, that provides image with greater magnification & projector lens allows greater magnification over intermediate lens. Both objective and projector lenses can provide excellent standard images through high power supply and highest stability to higher resolution standard.

In TEM Image-Recording System consist of fluorescent screen utilized for observing & focusing image. After observing the images, they were recorded constantly using digital camera. The collision of electrons by air molecules were prevented by a vacuum system. The vacuum system consists of guage, pump, valves & power supply will facilitate linear motion of electrons towards the image. Image thus formed is called monochromatic image. The obtained image may be recorded digitally & showed in computer & saved in JPEG/TIFF format. While storing, image could changed from their monochromatic to colored image on the basis of recording devices. By the use of pixel camera coloured image can be recorded & it is easy to visualize, identify & characterize the images [6].

4.3.4. Working Principle of Transmission Electron Microscope (TEM)

TEM works under the basis of light microscope. The light microscopes utilize light rays for targeting & producing the images but TEM exploits beam of electrons for targeting the sample & create the images. The wavelength of electrons i.e, 0.005 nm are100, 000 times shorter than light. Thus in case of resolution, TEM is 1000 times better than light microscope. In light microscope, the resolution power is inversely proportional to wavelength of light, while in TEM, resolution power is directly proportional to the wavelength of electron transmission due to the illumination of electron on the sample. TEM may used to detail internal morphology of tiny particles such as virion.

Figure 4.2: Photograph of TEM

Morphological and microstructural characterizations of the various materials were done by TEM (HRTEM, JEOL JEM 2100, Japan) of high-resolution. Specimens are coated on the carbon film using 200-mesh copper grid and a 200 keV voltage were accelerated to carry out the measurements. Sample preparation of TEM is carried out using sonicating powdered nanoparticle sample in an appropriate solvent. Carbon coated

copper grids were used for dispersion of the sample. The solvent solution was pipetted on grids for dispersion purpose. Electron microscopic analysis provides a clear and understandable evaluation of grain size, shape and particle distribution. Throughout the specimen, TEM guides a focused beam of electrons. TEM works under the principle of transmission of electrons & the produced images are much better than a light microscope.

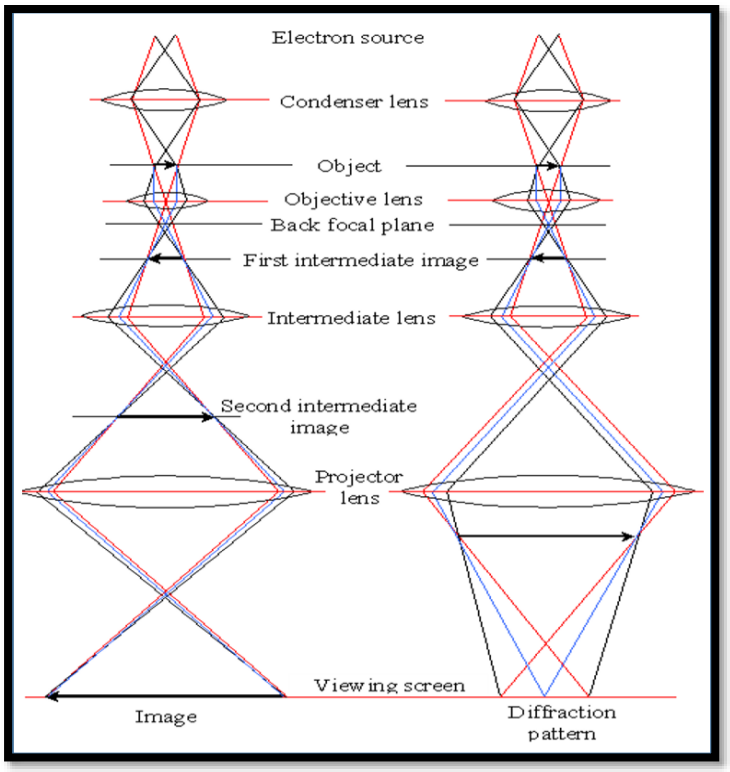

Figure 4.3: TEM ray diagram.

In TEM, electron beams having smaller wavelength are released by source of tungsten filament. The electron beams get transmitted while it falls on ultra-thin sample. Using objective lens, transmitted electron beam is targeted on CCD for creating an image. To create an image in TEM, resolving power increase with increase in wavelength of irradiation & gives information of crystal structure and size.

4.4. Scanning Electron Microscopy Technique

SEM is a device utilized for imaging & analyzing materials in various applications. SEM analysis is able to perform targeted areas on specimen & it can be utilized in qualitative/semi-quantitative determinations. It is utilized to produce high-resolution

images of shapes of objects (SEI) & to reveal spatial changes in chemical compositions [7] by obtaining elemental maps through EDS, phase discrimination on the basis of average atomic number & compositional maps.

4.4.1. Experimental set up for Scanning Electron Microscope

SEM consists of electron column, scanning system, detector, display, vacuum system & electronics control. The important parameters to perform the quality & resolution of SEM images were: instrument performance, selecting imaging parameters, sample nature.

The specimens may constant at a vacuum of 10^{-5} - 10^{-6} torr. The samples examined should be at higher vacuum because SEM performs at higher vacuum ~ 10^{-5} mbar. For this reason, liquids & watery materials should not examine directly. The finely powdered specimen might keep firmly on sample holder substrate then SEM specimen chamber may not be contaminated.

A typical electron microscope creates images of specimen through scanning by a focused electron beam is called as a SEM. The datas about surface topography & composition are obtained by creating signals through the interaction of electrons with atoms. Usually, electron beam is scanned in grid pattern & position of beam is attached using recorded signal to create the image. The better resolution obtained by SEM is 1 nm. Samples could examined at higher & lower vacuum, wet conditions & at broad area of cryogenic temperatures.

In SEM, the encouraged electrons carry significant quantity of kinetic energy, and this energy is dispersed into number of signals formed by electron-sample interactions. The signals consist of secondary electrons, backscattered electrons, diffracted backscattered electrons photons, visible light & heat [8].

Most common SEM mode is detecting secondary electrons released through atoms excited using electron beam. When the beam intersects the sample an angle is formed & thus number of secondary electrons was decided. Image of surface topography is formed through scanning specimen & collecting the secondary electrons emitted by special detector.

A SEM is a higher magnification microscope that utilizes targeted scanned electron beam having required top-down specimen formation & cross-sections for creating images of specimen. Usually, resolution of SEM image is lesser than TEM. Anyway, due to SEM image depends upon surface processes than transmission it is capable to image bulk specimens to cm in size. Images having better 3-D shape of specimen is formed depends on the settings & design of instruments.

4.4.2. Working Principle

The SEM device consists of electron column, sample chamber, EDS detector, electronics console & visual display monitor is shown in figure 4.2. Electron Gun, Electron Lenses, Sample Stage, Detectors for all signals of interest and Display / Data output devices are the important parts of SEM.

Electron source/gun emits the electron beam placed at the upper part of the instrument. Thermionic guns & Field emission guns are two varieties of electron guns utilized in SEM. Thermionic guns heats filament till the streaming of electrons. Through regulating strong electric field, Field emission gun splits away the electrons from their atoms. Microscope consists of stream of lenses inside the vacuum chamber. In order to increase efficiency, the electrons are pointed to the sample using those lenses. Magnification increases with the increase in electrons. The SEM utilizes pointed beam of electrons with high energy for producing various signals on sample surface.

SEM utilizes EDS & electron backscatterer diffraction set up. SEM provides the structural & elemental analysis of specimen. While the incident electron beam hits the sample, they release X-rays & 3 types of electrons: primary backscattered electrons, secondary electrons & Auger electrons. The interaction of primary electron beam on the specimen occurs in number of ways:

- Topographic nature of sample was identified using low energy secondary electrons produced from primary electrons.
- The images having higher degree of atomic number (Z) contrast are generated by the backscattering of primary electrons.

Primary backscatter electrons & secondary electrons are utilized by SEM. The X-ray emission or Auger electron ejection are happened due to the relaxation of ionized atoms through electron shell-to-shell transitions. When the electron beam passes through the microscope, the vacuum chamber prevent from the obstruction in SEM. The result can be obscured due to the defection of electrons by small particles. Usually SEM has secondary electron detectors & additional detectors. Ability of specific device depends on the aid of their detectors. The images are formed by the focusing of electron beam to a fine probe that scanned across the sample surface using scanning coils [9].

Figure 4.4 SEM Instrument

The imprint is recorded by an electron recorder using the rebounding electrons. To obtain three-dimensional images sharply these data are translated to a screen. The greatest advantage of SEM is their capability for repeating textual data into consistent & coherent manner. The data about topography & size of sample are not revealed by the electrons so traditional SEMs cannot form colour images. Anyway, current improvement made researchers for measuring energy trademarks in impact of incident beam to reaction of specimen.

4.5. Energy Dispersive X-Ray Analysis

An analytical method utilized for chemical characterization (presence of elements) of specimen is called as Energy-dispersive X-ray spectroscopy or energy dispersive X-ray analysis also named as energy dispersive X-ray microanalysis that depends on X-ray excitation source & specimen. The main principle of spectroscopy is that every element had particular atomic structures allow particular peaks in electromagnetic emission spectrum [10]. Energy dispersive spectrometer is provided with sample emitted X-rays & it calculates both intensity and energy of X-rays. Energy difference between two shells which is the element's characteristics occurs due to the electronic transition that is considered as energy of X-ray photon. Anyway, presence of elements in the specimen can be identified by calculating the wave lengths of X-rays emitted.

4.5.1 Experimental set up for Energy Dispersive X-Ray Analysis

Chemical structure of the prepared Co_3O_4 nanoparticles is shown in EDX profile. In EDX, localized chemical analysis is obtained by bombarding X-ray spectrum emission of solid specimen with targeted electron beams. Sample is fed with X-ray beam & then collision occurs. Finally, charged particles strikes from shells. The jumping of electrons from higher level to vacant shell results in the energy released to form X-rays called as Characteristic X-Rays. Wavelength of such X-rays depends on atomic number of element. The presence of elements in sample can determine by identifying wave lengths of X-rays emitted from sample. Qualitative analysis involves determination of spectral lines owing to typical X-ray spectra. Figure 4.3 shows the experimental arrangement of EDAX instrument [11].

4.5.2. Working Principle

The SEM with EDAX apparatus consists of 4 basic parts: Beam source, X-ray detector, Pulse processor, Analyzer

EDAX devices are mostly utilized by scanning electron microscopes & electron microprobes. SEM consists of cathode & magnetic lenses for producing & focusing electron beams. Selection of electron beam energy should satisfy the resolution requirements & efficiency of X-ray generation. X - ray radiation excited in sample were examined by completely focusing 2 crystal spectrometers. EDS X-ray detector calculates their energy Vs relative abundance of X-ray emissions. A lithium drifted silicon solid state device is regarded as a detector.

Figure: 4.5 EDAX instrument

A charge pulse proportional to X-ray energy was created while an incident X-ray beam knocks out the detector. Charge sensitive preamplifier converts charge pulse to voltage pulse. Pulses were arranged by voltage by sending signal to a multichannel analyzer. For exhibiting & data evaluation, energy identified from voltage measurement for all incident X-rays are send to a computer. To determine the elemental composition of specimen, X-ray energy versus counts were measured. EDAX cannot detect elements with low atomic number [12].

4.6. Fourier Transform Infrared Spectroscopy Techniques

FTIR Spectroscopy has led new applications in Infrared Spectroscopy. To identify the structures of molecules using characteristic absorption of infrared radiation is done by Infrared absorption spectroscopy. Fourier Transform is a mathematical algorithm. By using Fourier transform a raw data may be converted into spectrum & can examine vibrational transitions of molecules. FTIR spectrometers are advantageous in collecting spectral data & applied in organic synthesis, polymer science, petrochemical engineering, pharmaceutical industry & food analysis. When FTIR spectrometers are bridged to chromatography, then determination of unstable substances & mechanism of chemical reactions are achieved [13]. Experimental set up of FTIR instrument was given below in the Figure 4.4.

The Infrared region is classified as near-infrared region (12800-4000 cm^{-1}), mid-infrared region (4000-200 cm^{-1}) and far-infrared region (50-1000 cm^{-1}). Absorption radiation of organic & inorganic compounds is between (4000-400 cm^{-1}) so infrared absorption spectroscopy is utilized in this region & was a molecular vibrational spectrum. Change in dipole moment of specimen occurs then radiation of specific wavelengths absorbs while exposed to infrared radiation. As a result, the molecules transferring from ground state to excited state happens due to vibrational energy levels of sample. Vibrational energy gap determines the frequency of absorption peak. Number of absorption peaks of molecule was correlated with number of vibrational degrees of freedom. Change of dipole moment & ability for energy level transition depends on the intensity of absorption peaks.

Figure: 4.6. FTIR Instrument

4.6.1 Experimental set up for Fourier Transform Infrared Spectroscopy

4.6.2 Working Principle

Characterization of FTIR spectra for pure & doped Co_3O_4 nanoparticles were done by using IR Affinity1, Shimadzu make FTIR Spectrometer. Infrared light is used to scan & examine chemical properties of sample in FTIR analysis [14]. FTIR measurement in the wave number between 400 - 4000 cm^{-1} was utilized for determining the biomolecules accountable for reduction of the Co^{+} ions.

Spectrophotometry was utilized to determine the equilibrium constant of solution. In some solutions, reaction occurs in both forward & reverse directions such as reactants into product & products break down to reactants. Equilibrium point is the point where this chemical reaction meets a point of balance. Light transmittance of solution may be tested by spectrophotometry for examining the concentrations of reactants & products equillibrium point. Schematic diagram of FTIR instrument is figured on Figure 4.5.

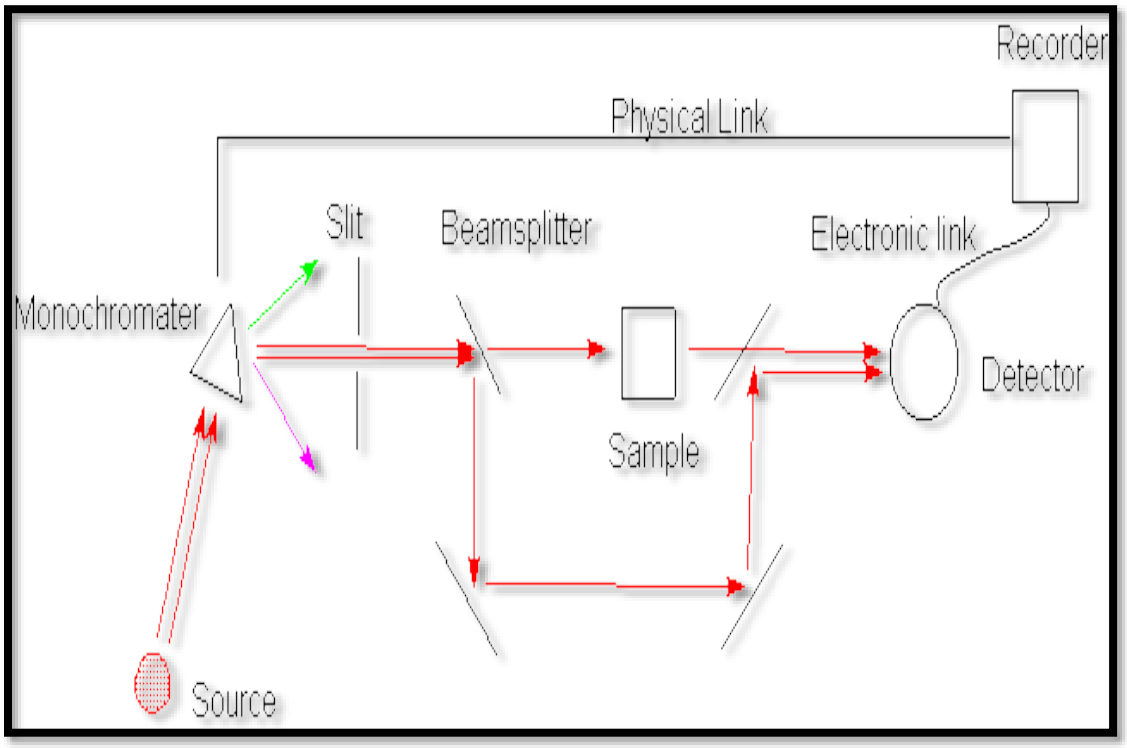

Figure: 4.7 Schematic diagram of a FTIR instrument

Specimens for IR spectrophotometry are coated between two discs of potassium bromide & crushed to a pellet. For measuring aqueous solutions, insoluble silver chloride was utilized to build cell. The analytical spectrum in spectrophotometers is generated by monochromator having diffraction grating. Grating may be movable / fixed. Light intensity at every wavelength can be detected by scanning stepwisely through grating. A Fourier transform technique utilizes latest mid-infrared spectrophotometers to obtain spectral information & is named as FTIR spectroscopy [15].

The interferometer is fundamentally different from a monochromator. Change in energy Vs time concurrently at all wavelengths is a unique way to record spectra is

reported by the detector. To provide a reference for device operation a laser beam is superimposed. However, time & frequency are reciprocals we can determine their relationship.

Fourier transform, a function of mathematics converts an intensity vs time to intensity vs frequency spectrum is accurately designed device but have various limitations. Firstly, amount of signal is limited by monochromator/slit for targeted resolution. Secondly, lack of multiple scans to generate signal-to-noise ratios. Lastly, repeated calibration of device is needed due to analogous relation between monochromator position & recording device based on misalignment & wear [16].

4.7. UV-Visible Spectroscopy

The Ultraviolet-visible spectroscopy referred to absorption/reflectance spectroscopy in the UV-visible spectral region having wavelength between 0.39-0.77 μm & it straightly depends on observed color of the chemicals sophisticated. Due to the upgrading of electrons from ground state into excited state, the UV (Ultra-Violet) spectroscopy is called as Electronic spectroscopy. In this region, atoms & molecules experience electronic transitions.

Quantitative examination for various analytics like transition metal ions, heavily conjugated organic compounds & biological macromolecules are analyzed by UV/Vis spectroscopy [17]. Typical spectrophotometers utilized in UV & visible regions of spectrum can also perform in the near-infrared region. Spectrophotometers could neither single nor double beam.

4.7.1 Experimental set up for UV-Visible Spectroscopy Analysis

UV-Visible spectroscopy is a method utilized to quantify light by absorbing & scattering through specimen. On its simplest form, specimen is kept between light source & photodetector. Before & after travelling into specimen the intensity of beam of light is calculated. A typical UV-Visible spectrophotometer is given below in the figure 4.6.

The molecules having π/n-electrons absorbed the energy through ultraviolet /visible light to promote electrons to higher anti-bonding molecular orbitals. Generally, more encouraged transition is from the highest occupied to lowest unoccupied molecular orbital. On the whole spectra solution obeys Beer-Lambert law [18]:

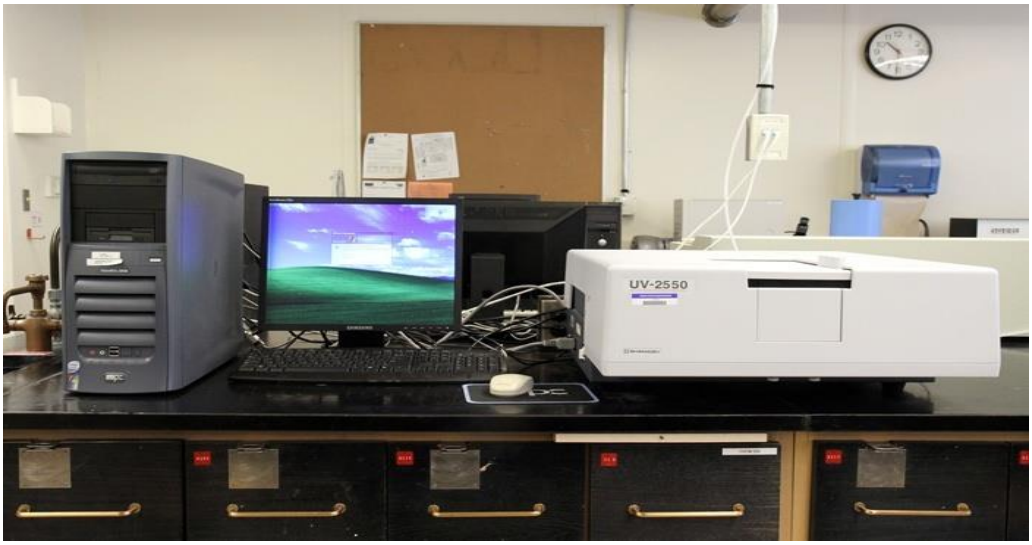

Figure: 4.8. UV-Visible Spectrophotometer

Beer-Lambert law states that greater number of molecules able for absorbing light of given wavelength is greater extent of light absorption is the fundamental principle of UV spectroscopy. Beer-Lambert law is expressed as:

$$A = \log (I_0/I) = Ecl$$

Here, A = absorbance, I_0 = intensity of light incident on specimen, I = intensity of light leaving specimen, c = molar concentration of solute, l = length of specimen (cm) E = molar absorptivity.

Beer-Lambert Law is utilized for characterizing various compounds. The Beer-Lambert law states that the absorbance of a solution is directly proportional to the concentration of the absorbing species in the solution and the path length [6]. For a fixed path length, UV/Vis spectroscopy is utilized to examine the concentration of absorber in a solution. By removing the concentration dependence, extinction coefficient (ε) is measured as a function of wavelength. Device utilized for determining the ratio of intensity of two beams of light in UV-Visible region is called as Ultraviolet-Visible spectrophotometers. An ultraviolet spectrophotometer measures the intensity of light passing through a sample (I) and compares it to the intensity of light before it passes through the sample (I_0). The ratio (I/I_0) is called the transmittance, and is usually expressed as a percentage (%T).

The absorbance, A, is based on the transmittance: A = -log (%T/100%) [19].

4.7.2 Working Principle

A UV/Vis spectrophotometer is the device utilized in ultraviolet-visible spectroscopy to measure the quantity of ultraviolet or visible radiation absorbed by a substance in solution. Schematic diagram of UV-Visible spectrophotometer is shown in the figure 4.7.

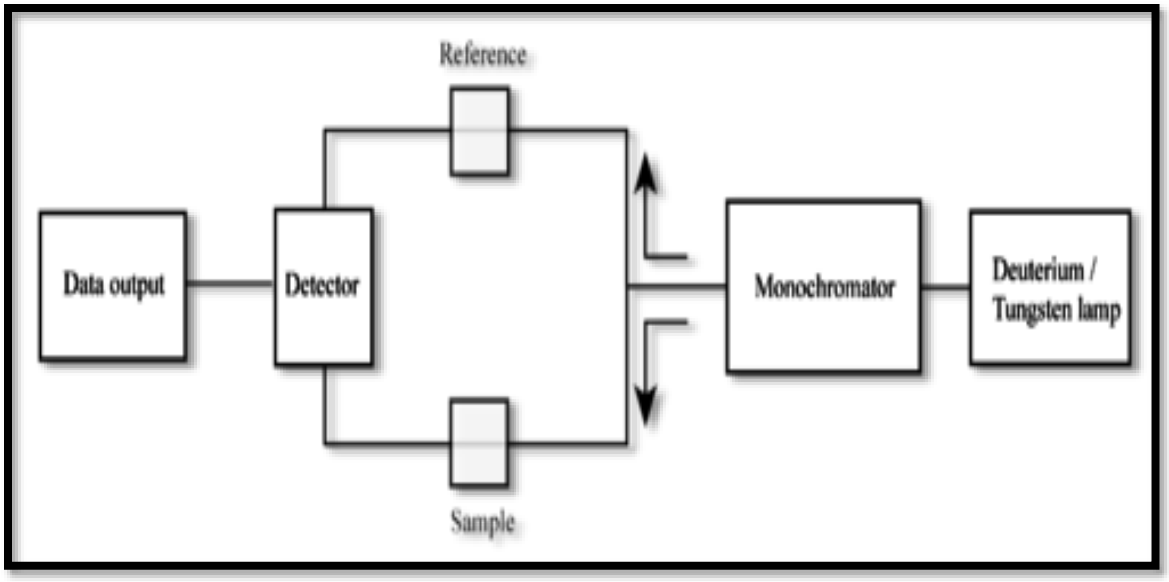

Figure: 4.9 Schematic diagram of a UV-Visible spectrophotometer

UV-visible spectrophotometers are used to calculate reflectance. Here, spectrophotometer calculates the intensity of light reflected from a sample (I), and compares with intensity of light reflected from a reference material (I_0). This ratio (I/I_0) is called reflectance, & commonly expressed as percentage. Basic parts of a spectrophotometer are: light source, sample compartment, monochromator, detector & recording devices.

The light source such as Tungsten filament (300-2500 nm), deuterium arc lamp, that is constant at ultraviolet region (190-400 nm), Xenon arc lamp, continuous from 160-2,000 nm Recently, light emitting diodes (LED) as the radiation source for the visible wavelengths. Monochromators generally consists of prisms & slits. Rotating prisms splits the radiation emitted by primary source. Different wavelengths of light source splited by prism were chosen by slits so the rotation of prism results in continuous constantly enhancing wavelengths for recording purposes to pass through the slits.

Sample compartment contains cell holders- Sample cells and reference cells. Sample & reference solutions are kept in cells. Glass cannot be utilized for cells because it absorbs light in the UV region so cells are made of either silica or quartz. Light beams enter into the sample compartment & passes through the detector that is the final element in spectrophotometer. Usually, in UV spectroscopy two photocells perform the function of detector. Firstly, photocells accepts beam from sample cell & second detector accepts beam from the reference. Intensity from radiation of reference cell is greater than the beam from the sample cell. Then, formation of pulsating or alternating currents in the photocells is occured.

A silicon photodiode is a detector which utilizes the electrical properties of detector change while it is exposed to light. Most of the time amplifier is connected to a pen recorder that coupled to the computer. Alternating current produced in photocells is converted into amplifier & then it is matched to a small servo meter. Usually low intensity current is produced in the photocells. A clear & recordable signal is obtained by an amplifier that amplifies the signals for various times. A spectrum of desired compound is produced by generating all the datas stored in computer [20].

4.8. Results and Discussion

4.8.1 X-Ray Diffraction Analysis

X- ray diffraction images of synthesized pure & 3%, 5%, 10% of Zn, Fe, Cu and Ni doped Co_3O_4 nanoparticles are shown in figure 4.8. Crystalline nature of prepared nanoparticles is indicated by highly intense, prominent & sharp diffraction peaks in XRD pattern.

For pure Co_3O_4 nanoparticles sharp diffraction peaks conformed the formation crystalline structure are found at 2θ values of19.08^0, 37.6^0, 44.7^0, 59.4^0, and 65.2^0 corresponding to the (111), (311), (400), (511) and (440) planes. According to JCPDS card number (14-0673) all these peaks correspond to spherical shaped Co_3O_4 nanoparticles [21].

Sharp diffraction peaks observed at 2θ values of 31.3^0, 37.6^0, 44.7^0, $59.4^0$and 65.2^0 corresponding to the (220), (311), (400), (511) and (440) planes respectively attributed to the doped Co_3O_4 nanoparticles & are in accordance with JCPDS card

number (89-0511). The presence of the new plane at (220) confirmed the presence of the dopants. These diffraction peaks can be indexed to the crystalline cubic phase Co_3O_4 with lattice constants of a = 8.036 Å, that agreed with the reported values (JCPDS card no. 76-1802). Lattice strain induced by oxygen vacancies are due to small variation in lattice parameter.

Table 4.1. Average crystallite size of pure and doped Co_3O_4 nanoparticles

Material	D = 0.89λ/βCosθ (nm)
Co_3O_4 nanoparticles	37
3% of Zn doped Co_3O_4 nanoparticles	39
5% of Zn doped Co_3O_4 nanoparticles	40
10% of Zn doped Co_3O_4 nanoparticles	41
3% of Fe doped Co_3O_4 nanoparticles	37
5% of Fe doped Co_3O_4 nanoparticles	38
10% of Fe doped Co_3O_4 nanoparticles	39
3% of Cu doped Co_3O_4 nanoparticles	46
5% of Cu doped Co_3O_4 nanoparticles	47
10% of Cu doped Co_3O_4 nanoparticles	48
3% of Ni doped Co_3O_4 nanoparticles	41
5% of Ni doped Co_3O_4 nanoparticles	42
10% of Ni doped Co_3O_4 nanoparticles	43

Using Debye-Scherrer formula [D = 0.89 λ/ β Cos θ] crystallite size of material had been determined on the basis of FWHM highly intense peak & is shown in table 4.1. For pure Co_3O_4 nanoparticles average crystallite size is around 37 nm. Because of lower solubility of dopants in CoO matrix a narrow increase in crystallite size of doped sample is observed. Possibility of secondary impurity phase decreases because doped concentration is under the solubility limit of dopant in CoO matrix. High purity of the samples was conformed due to the lack of diffraction peaks regarding impurities in X-ray spectra. Patterns achieved from XRD are in accordance with earlier reports [22].

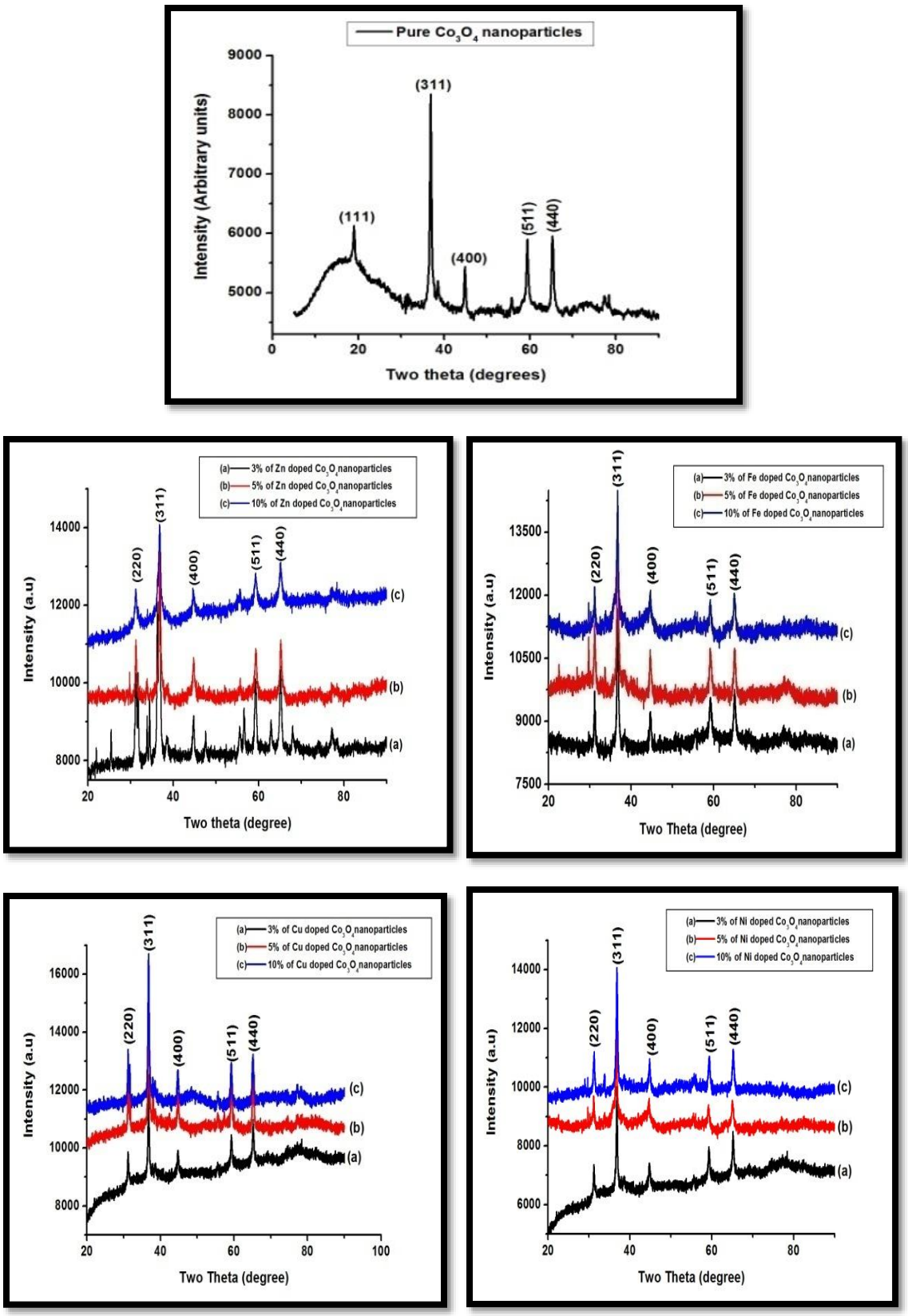

Figure: 4.10 XRD Pattern of pure and doped Co_3O_4 nanoparticles

4.8.2. Transmission Electron Microscope Analysis

For synthesized pure & doped Co_3O_4 nanoparticles their morphology & microstructure were investigated by the use of TEM analysis & are shown in Figure 4.9.

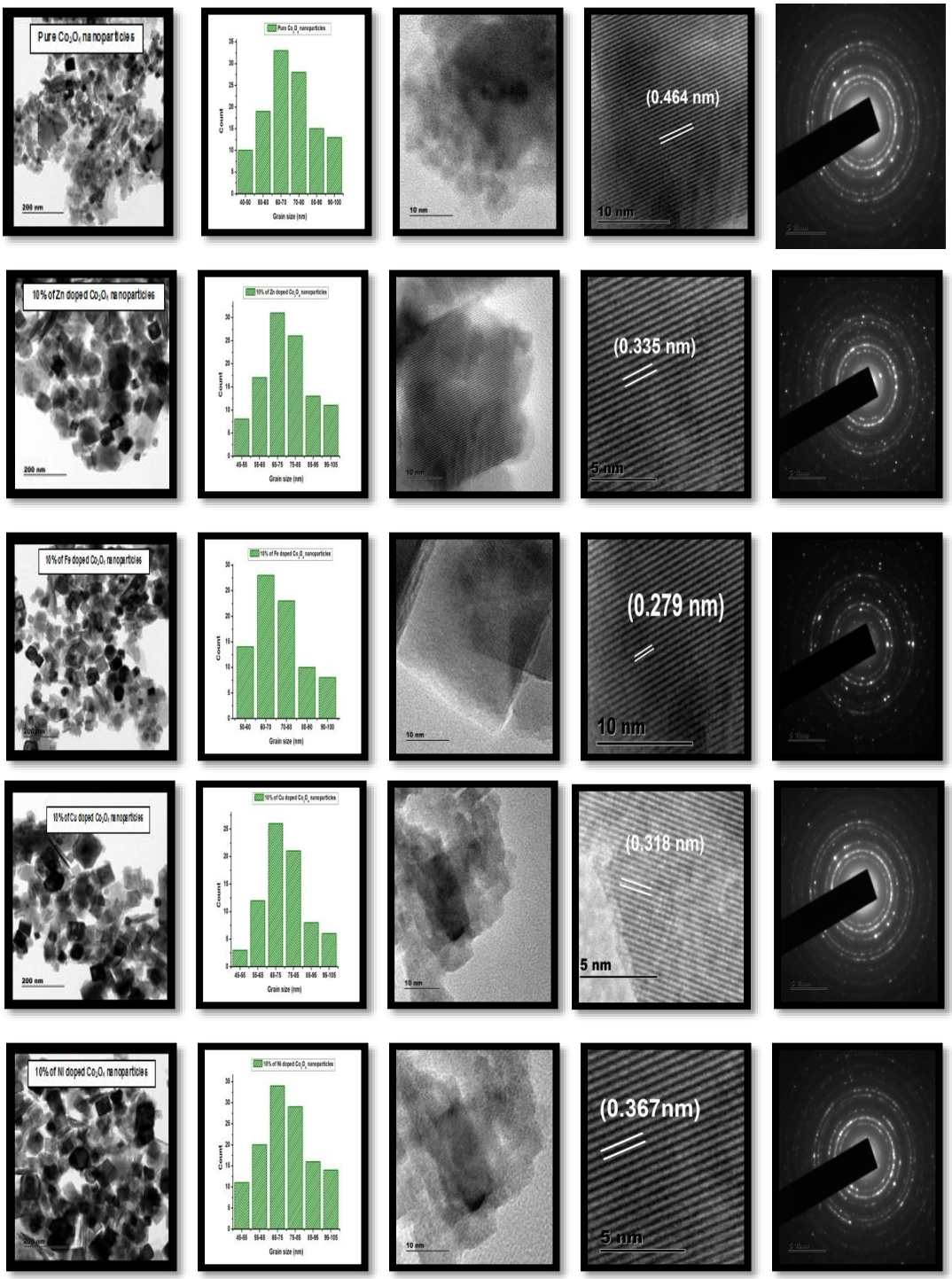

Figure: 4.11 TEM images & SAED patterns of pure and doped Co_3O_4 nanoparticles

The grain size of sample is measured by the use of Image j software from different TEM images and grain size was found between 60 nm and 80 nm. The grain size obtained from TEM analysis is greater than the crystallite size measured from XRD.

The SAED pattern confirms the crystallinity of samples. It contains more diffraction rings which show that crystallinity of sample is high. It indicates the presence of more than one crystallite in a particle. Sample is characterized by diffraction rings having discrete spots determines the crystallinity of sample having polycrystalline nature. For pure & doped Cobalt oxide nanoparticles layer separations are observed approximately at 0.464 nm, 0.335 nm, 0.279 nm, 0.318 nm, 0.367 nm. Spotty rings in SAED patterns reflect the polycrystalline nature of the samples. The interplanar distance measured from HRTEM images match well with the spacing corresponding to prominent planes in the XRD spectrum [23].

4.8.3. Scanning Electron Microscope Analysis

For pure & doped Co_3O_4 nanoparticles the scanning electron micrograph images are exhibited on Figure4.10. Micrograph images clearly show well dispersed spherical Cobalt oxide nanoparticles. The 3%, 5% and 10% of doped Co_3O_4 nanoparticles are observed to have lower agglomeration than pure Co_3O_4 nanoparticles. Among the doped ones, Co_3O_4 nanoparticles doped with 10% of Fe have the least agglomeration. Overall nucleation & coagulation of every nanoparticles determines the morphological characteristics of the samples [24].

The particle size was examined and was found to be between 40nm-120nm for pure and doped Co_3O_4 nanoparticles. By the use of Image J software, size distribution of Co_3O_4 nanoparticles was determined & an average diameter is found to be 95 nm.

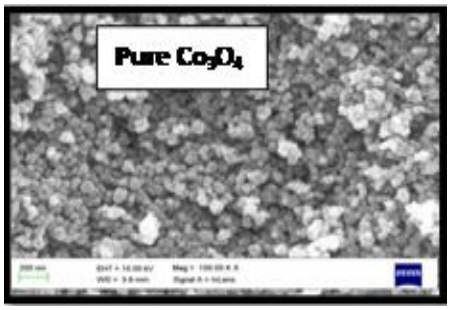
Pure Co_3O_4

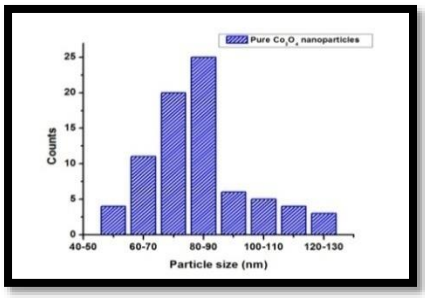
Pure Co_3O_4 nanoparticles
Counts
Particle size (nm)
40-50
60-70
80-90
100-110
120-130

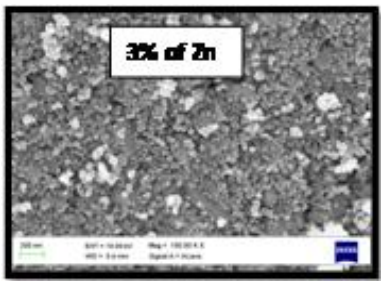
3% of Zn

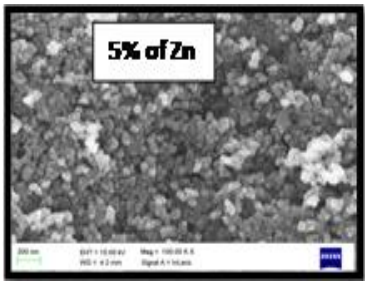
5% of Zn

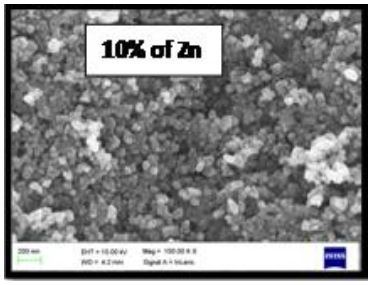
10% of Zn

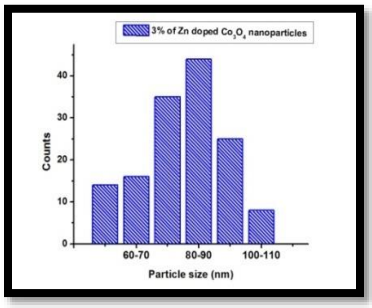
3% of Zn doped Co_3O_4 nanoparticles
Counts
Particle size (nm)
60-70
80-90
100-110

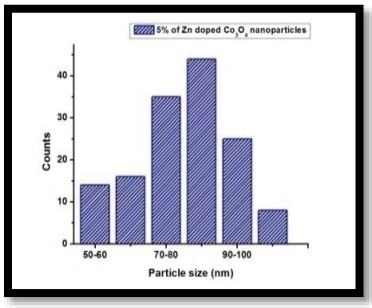
5% of Zn doped Co_3O_4 nanoparticles
Counts
Particle size (nm)
50-60
70-80
90-100

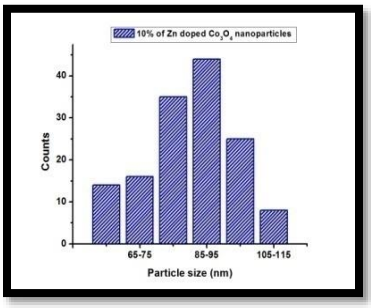
10% of Zn doped Co_3O_4 nanoparticles
Counts
Particle size (nm)
65-75
85-95
105-115

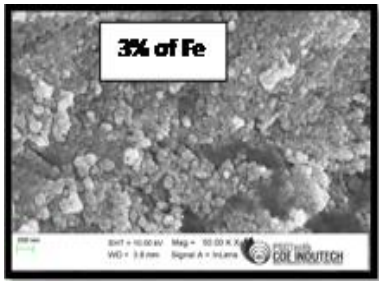
3% of Fe

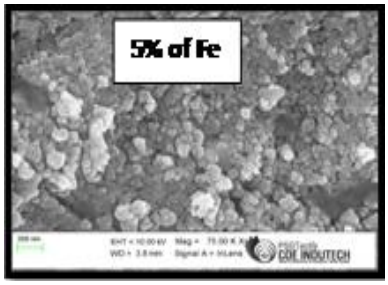
5% of Fe


10% of Fe

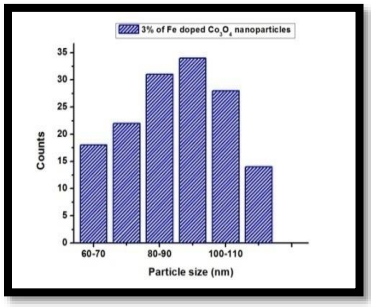
3% of Fe doped Co_3O_4 nanoparticles
Counts
Particle size (nm)
60-70
80-90
100-110

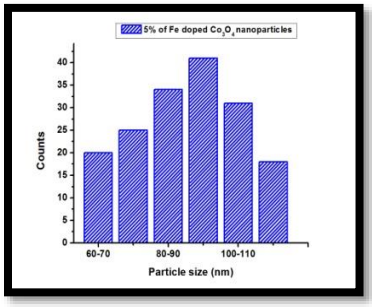
5% of Fe doped Co_3O_4 nanoparticles
Counts
Particle size (nm)
60-70
80-90
100-110

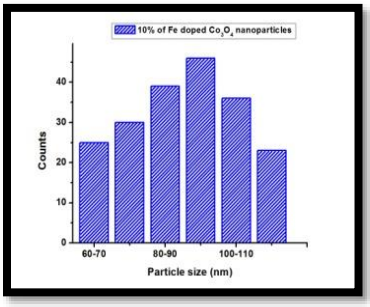
10% of Fe doped Co_3O_4 nanoparticles
Counts
Particle size (nm)
60-70
80-90
100-110

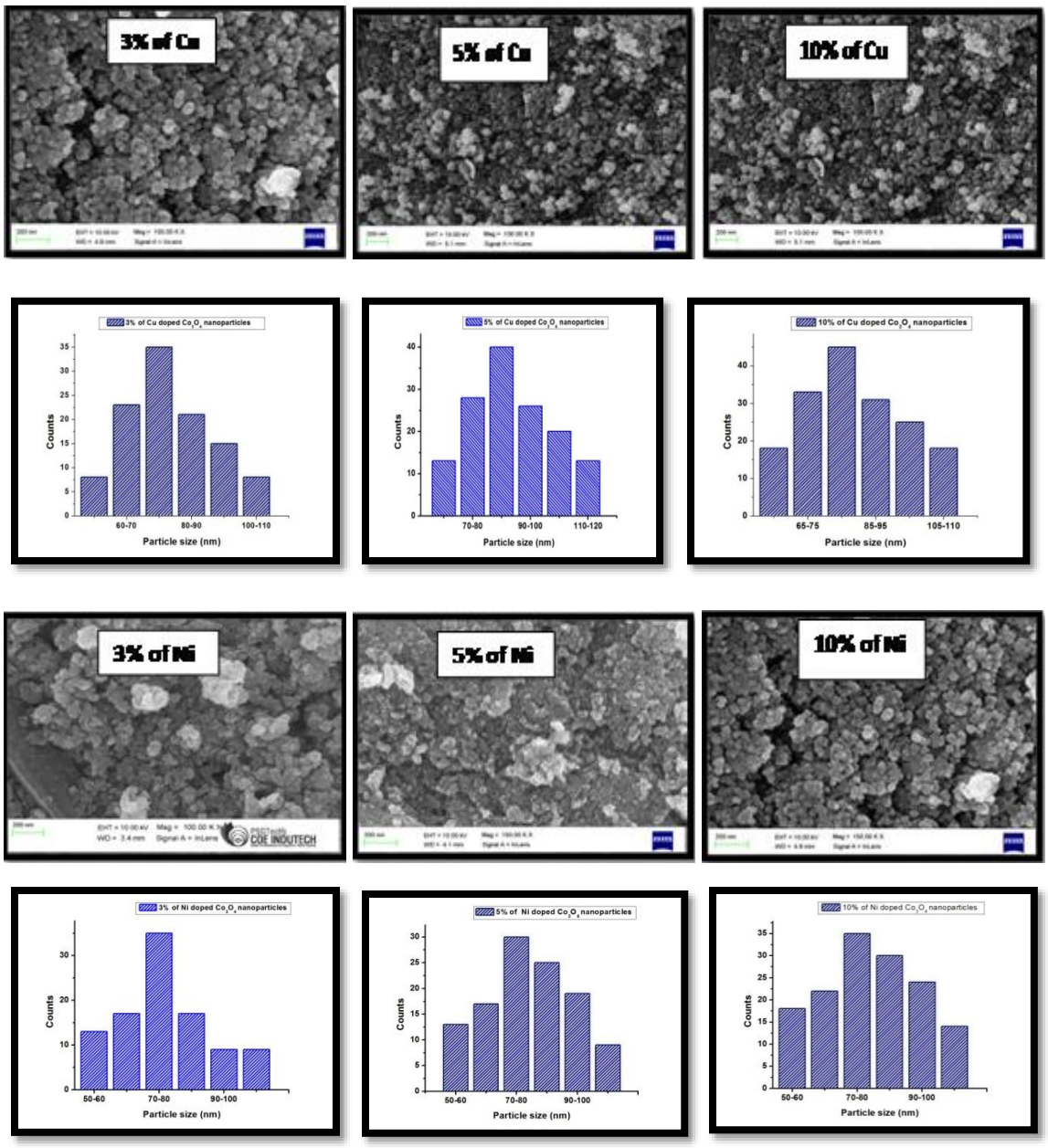

Figure: 4.12 SEM and particle size images for different concentrations of pure and doped Co_3O_4 nanoparticles

4.8.4. Energy Dispersive X - Ray Spectrum Analysis

EDX spectrum confirmed the existence of Cobalt and Oxygen with Zn, Fe, Cu, Ni elements and the Atomic and Weight percentage are revealed on figure 4.11. The dispersive energy values correspond to 0.5, 0.8, 1.1, 6.9 and 7.6KeV.

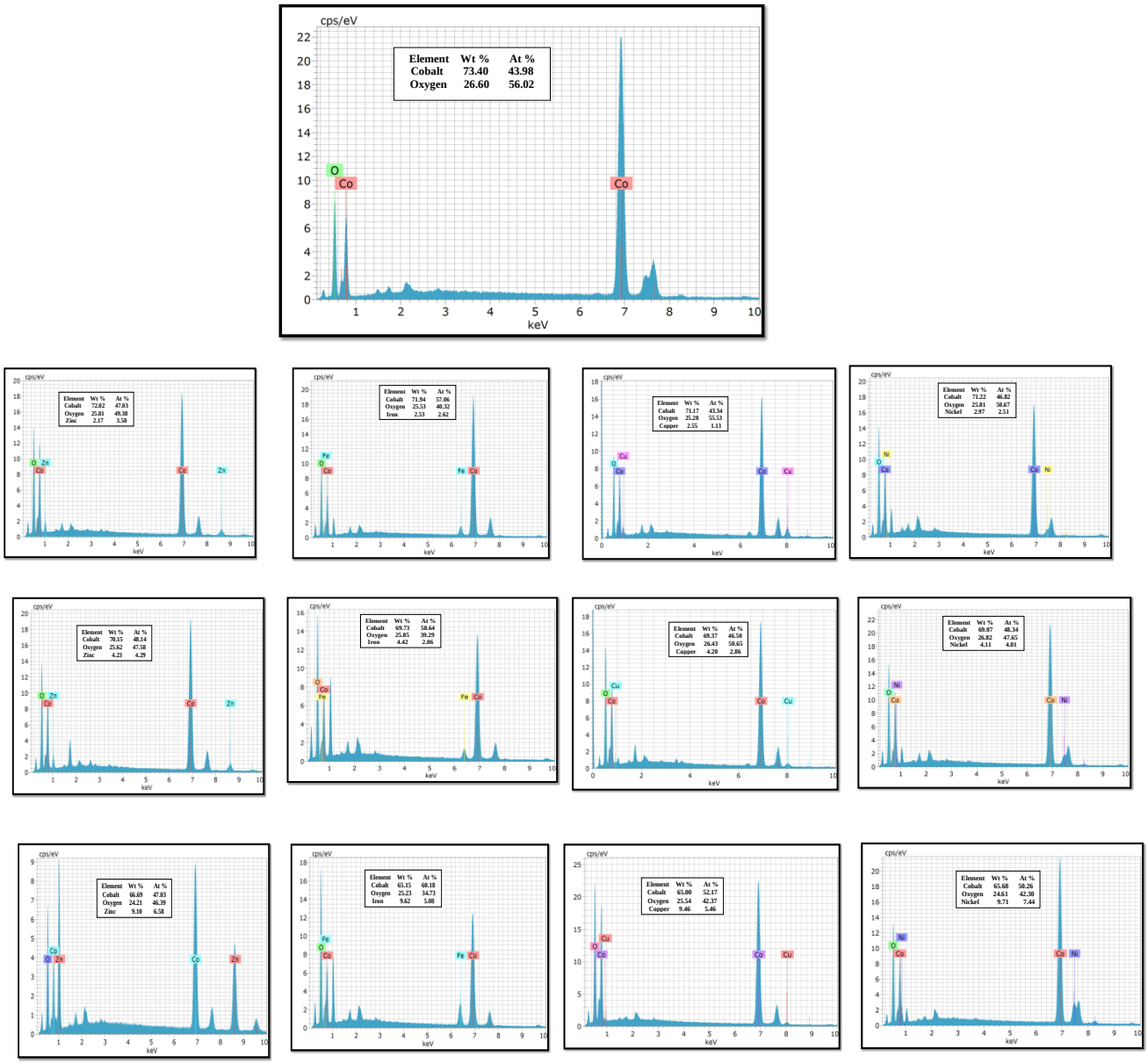

Figure: 4.13 EDAX spectra of pure and doped Co_3O_4 nanoparticles

EDX spectra of synthesized pure, 3%, 5% and 10% of Zn, Fe, Cu and Ni doped Co_3O_4 nanoparticles are shown in figure 4.11. EDX spectroscopy is used to determine the atomic and weight percentages of the elements present in the sample. It is found that all the samples were rich in cobalt and oxygen element along with small amounts of Zn, Fe, Cu and Ni. EDX spectrum established the appearance of Co and O elements having dispersive energy values corresponds to 0.9, 2.2, 8.5, 9.6 KeV [25]. Purity of sample was confirmed with the absence of other peaks regarding other components.

4.8.5 Fourier Transform Infrared Analysis

The existence of functional groups for pure & doped Cobalt oxide nanoparticles were determined by FTIR analysis. In figure 4.12, FTIR spectra of pure & doped Co_3O_4 nanoparticles were shown in the investigated region (4000–400 cm^{-1}). Absorption peaks were found around 3210 cm^{-1}, 1636 cm^{-1}, 1540 cm^{-1}, 1370 cm^{-1}, 851 cm^{-1} and 644.79 cm^{-1} [26].

Absorption bands at 851 cm^{-1} & 644.79 cm^{-1} arises from stretching vibrations of metal-oxygen bond (Co-O), established the generation of Co_3O_4 nanoparticles. Broad band centered at 3210 cm^{-1} & peaks at 1636 cm^{-1} were individually alloted to OH-stretching and bending vibration modes of the water molecules adsorbed. Peaks at 1370 cm^{-1} & 1540 cm^{-1} were committed to Co-O-H vibrations.

The modification of peaks in FTIR spectrum occurs by adding dopants. A sharp peak observed at 872 cm^{-1} in spectrum is attributed to the dopant-Oxygen bond generation. Adsorbed water molecules showed absorbance peaks between 800 cm^{-1} - 1200 cm^{-1} as the nanocrystalline materials maintain moisture. Metal oxygen frequencies viewed for respective metal oxides agree with early results [27].

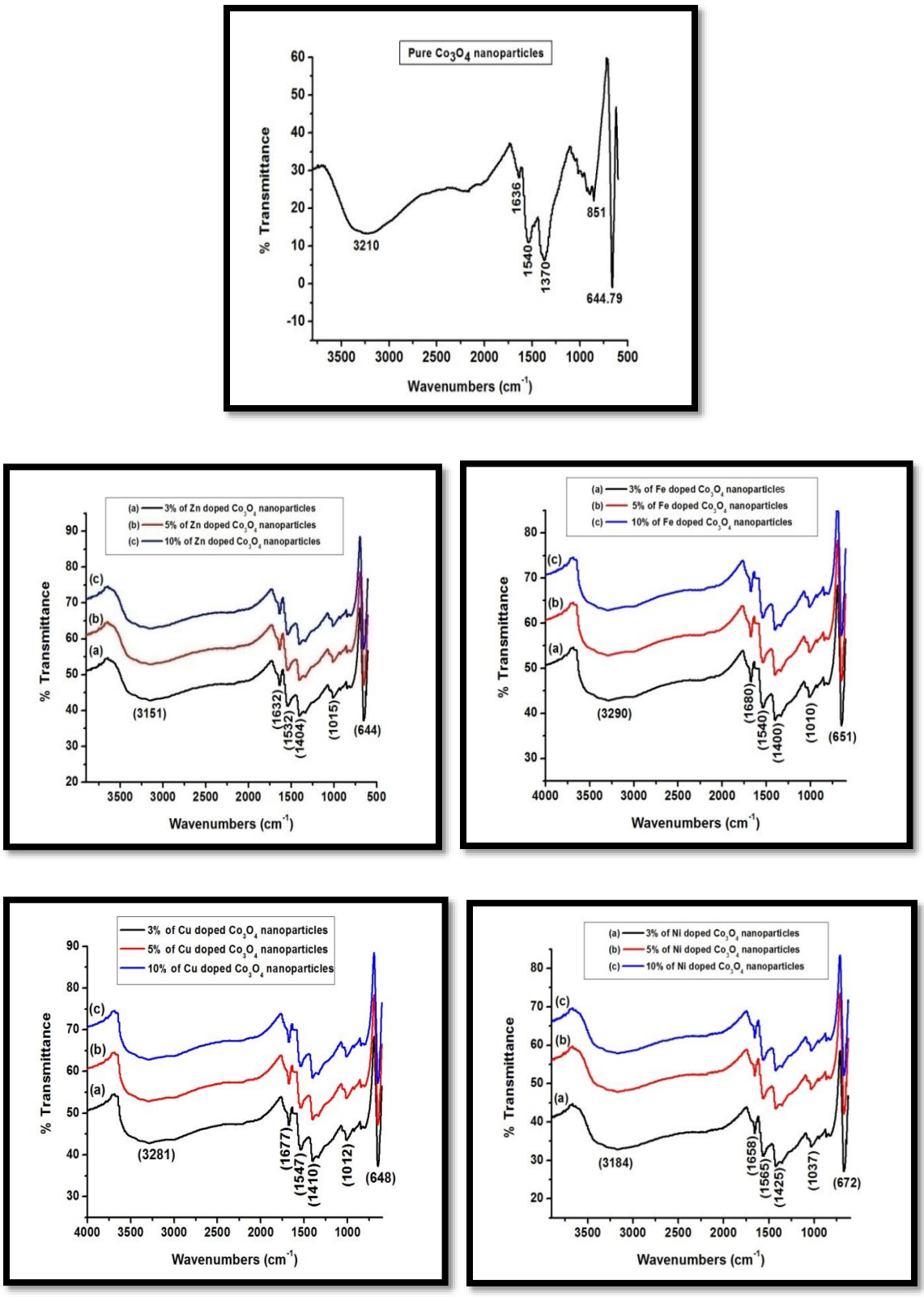

Figure: 4.14 FTIR spectra of Co_3O_4 nanoparticles

4.8.6 UV-Visible Spectroscopy Analysis

Optical properties of synthesized Co_3O_4 nanoparticles were characterized by UV-visible spectrophotometer. Characterization of absorption peak is performed by UV-visible spectroscopy by Cyber lab UV-100 spectrophotometer from 350 nm to 800 nm. Optical absorption characteristics of pure & doped Co_3O_4 nanoparticles were found in Figure 4.13. A peak at 23 nm is observer for pure cobalt oxide. The wide absorption peaks found above 263 nm attributes for accumulating dopants at surface of Co_3O_4 nanoparticles. The ligand to metal charge transfer O – Co was confirmed by solid absorption band in UV light. Bandgap energy values were calculated for pure & doped Co_3O_4 nanoparticles and are tabulated in table 4.2 using Tauc plot relation.

$$(\alpha h\upsilon)^{\gamma} = A\,(h\upsilon - E_g)$$

Where A is the absorbance, α is the absorption coefficient, hυ is the incident photon energy, E_g is the bandgap energy and n=1/2 and 2 for direct and indirect bandgap respectively.

As the crystallite size decreases the energy gap increases due to the lower impurity concentration. It is a consequence of the charge carrier movement confinement in a limited space. The results obtained in the present examination are in acceptable concurrence with prior investigations [28, 29].

Table 4.2. Bandgap energies for pure and doped Co_3O_4 nanoparticles

Material	Bandgap energy (eV)
Co_3O_4 nanoparticles	2.03
3% of Zn doped Co_3O_4 nanoparticles	2.15
5% of Zn doped Co_3O_4 nanoparticles	2.14
10% of Zn doped Co_3O_4 nanoparticles	2.13
3% of Fe doped Co_3O_4 nanoparticles	2.09
5% of Fe doped Co_3O_4 nanoparticles	2.08
10% of Fe doped Co_3O_4 nanoparticles	2.07
3% of Cu doped Co_3O_4 nanoparticles	2.13
5% of Cu doped Co_3O_4 nanoparticles	2.12
10% of Cu doped Co_3O_4 nanoparticles	2.11
3% of Ni doped Co_3O_4 nanoparticles	2.18
5% of Ni doped Co_3O_4 nanoparticles	2.17
10% of Ni doped Co_3O_4 nanoparticles	2.16

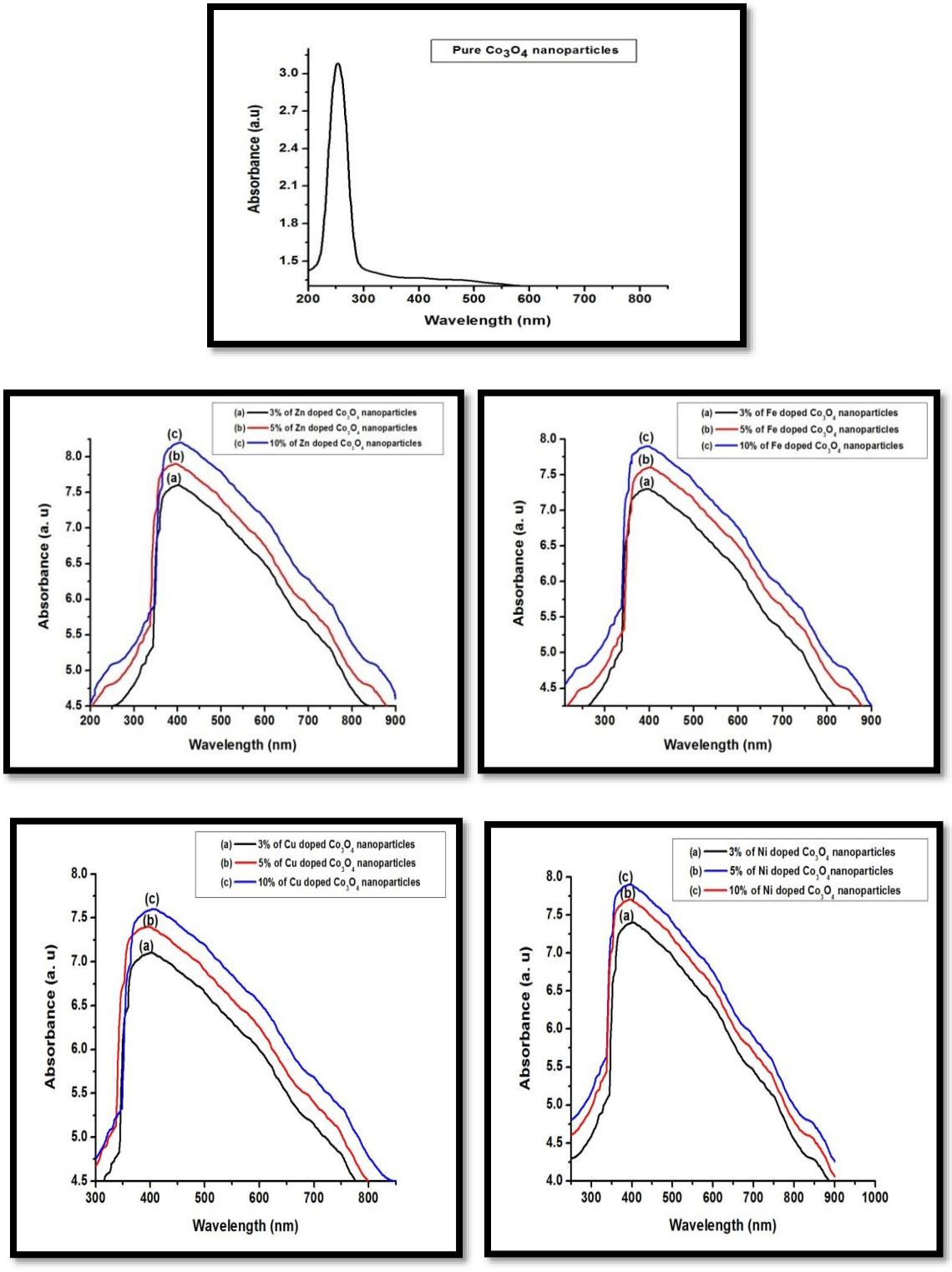

Figure: 4.15 UV - Vis Spectrum of pure and doped Co_3O_4 nanoparticles

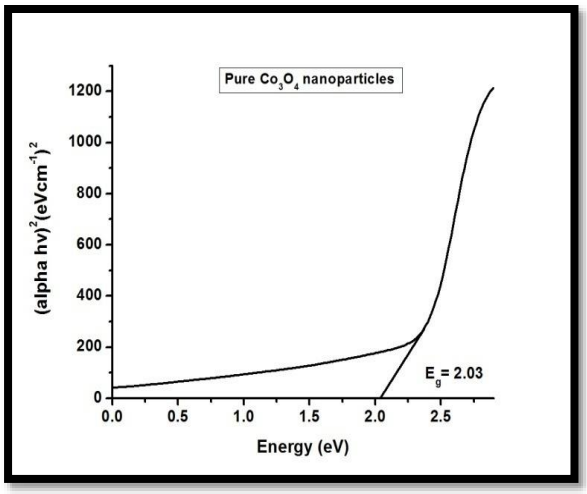

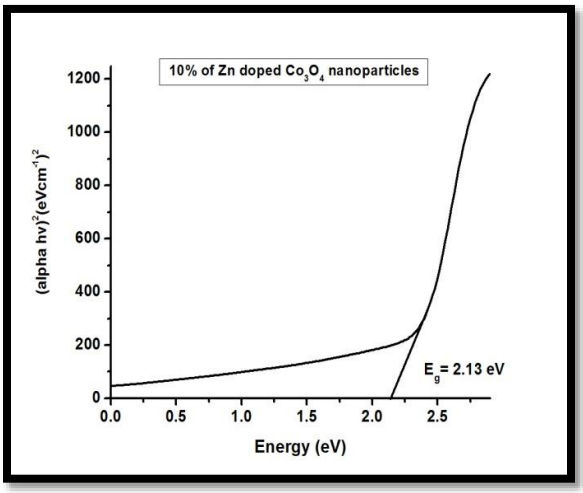

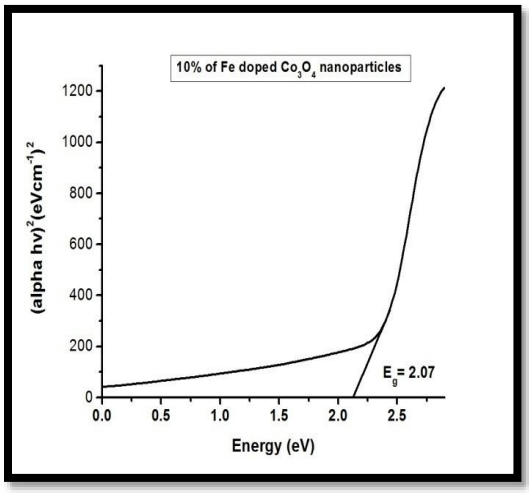

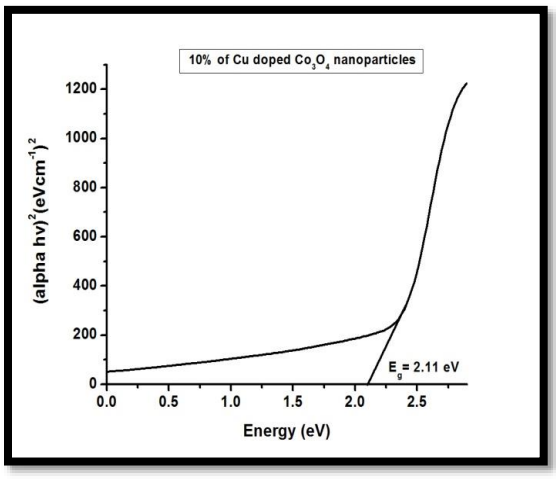

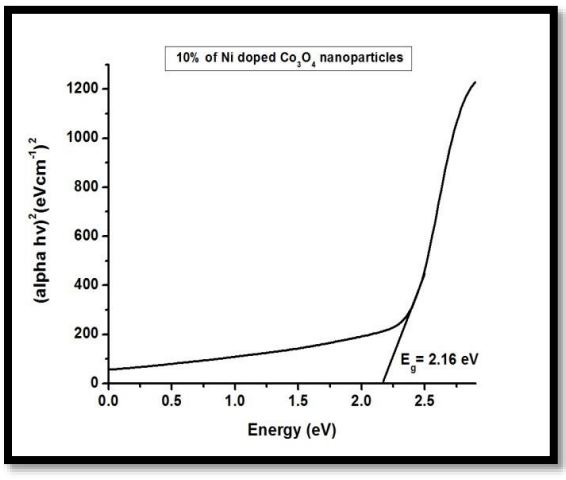

Figure 4.15(a) Bandgap energy values for pure & 10% of Zn, Fe, Cu and Ni doped Co_3O_4 nanoparticles

4.9. Conclusion

The Co_3O_4 nanoparticles are synthesized by the use of low-cost hydrothermal method. XRD analysis confirms that Co_3O_4 nanoparticles are profoundly crystalline in nature. The grain size was found using TEM analysis. Particle size affirmed by SEM examination was spherical in structure. EDAX spectrum affirms the existence of Zn, Fe, Cu, Ni, Co & O components with no other foreign elements. Presence of the bioconstituent elements attached to surface of Co_3O_4 nanoparticles is confirmed from FTIR examination. UV spectroscopic investigation shown a strong absorption peak around 263 nm and its bandgap energy were also calculated. Overall results obtained from different characterization techniques confirm the presence of metal ions for their various applications.

References

[1] Pandey, A., Dalal, S., Dutta, S., & Dixit, A, Journal of Materials Science: Materials in Electronics, 32 (2021) 1341-1368.

[2] Boddolla, S., Thodeti, S, International Journal of Engineering, Science & Mathematics, 7 (2018) 169-175.

[3] Yousefi, A., & Nezamzadeh-Ejhieh, A, Iranian Journal of Catalysis, 11 (2021) 247-259.

[4] Mertens H. D, Svergun D. I, Archives of biochemistry and biophysics, 628 (2017) 33-41.

[5] Hansel, C. S., Holme, M. N., Gopal, S., & Stevens, M. M, Biomaterials, 226 (2020) 119406.

[6] Kannan M, A textbook on fundamentals & applications of nanotechnology (2018) 93-102.

[7] Reddy, P, Journal of Innovation in Mechanical Engineering, 2(2019) 28-31.

[8] Inkson, B. J. In Materials characterization using nondestructive evaluation (NDE) methods (2016). Woodhead publishing. 17-43.

[9] Hii, S. Y. (2011). Physical and chemical properties of vanadyl pyrophosphate catalysts obtained via different calcination temperatures (Doctoral dissertation, UTAR).

[10] Haschke, M. (2014). Laboratory micro-X-ray fluorescence spectroscopy (Vol. 55). Springer.

[11] Noor, S. M., Mei, C. S., Ibrahim, et al, InIOP Conference Series: Earth and Environmental Science 220 (2019) IOP Publishing. 012024.

[12] Scimeca, M., Bischetti, S., Lamsira, H. K., Bonfiglio, R., & Bonanno, E. European journal of histochemistry: EJH, 62 (2018).

[13] Lin, S. Y., Critical Reviews in Solid State and Materials Sciences, 41(2016) 482-530.

[14] Hou, X., Lv, S., Chen, Z., & Xiao, F, Measurement, 121 (2018) 304-316.

[15] Okere E.E., Arendse, E., Nieuwoudt H., Perold, W. J., Opara, U. L., Frontiers in Plant Science, 13 (2022).

[16] Goda, K., & Jalali, B., Nature Photonics, 7 (2013) 102-112.

[17] Nejati-Yazdinejad, M., & Kakeh, F., Arabian Journal of Chemistry, 10 (2017) S2518-S2522.

[18] Casasanta, G., Falcini, F., & Garra, R., Journal of Photochemistry and Photobiology A: Chemistry, 432 (2022) 114086.

[19] Zhao, J., & Cheng, Y., Advanced Theory and Simulations (2022) 2200520.

[20] Ahmed, S.A. E., Mohammed, T. A. E., Ahmed, A. M. M, Nucl. Radioact. Phys., 106 (2017) 46802-46805.

[21] G. Pandey, S. Dixit, J. Phy. Chem. C. 115 (2011) 17633-17642.

[22] S. Laurent, D. Forge, et al., Chem. Rev. 108 (2008) 2064-2110.

[23] Manjunath, K., & Thimmanna, C. G. Materials Research Express, 5 (2018) 035030.

[24] Soundararajan Stella, Ramachandran, AIP Adv, 5 (2015) 087104.

[25] L. Liu, et al., J. Power Sources, 327 (2016) 135-144.

[26] Weidong Zhang, Paola Anguita, et al., Catalysts, 10 (2020) 865.

[27] Rasayan, J. Chem. 11 (2018) 88–102.

[28] Farhadi, et al., Acta Chim. Slov. 63 (2016) 335–343.

[29] R.N. Mariammal, K. Ramachandran, et al., Appl. Surf. Sci. 270 (2013) 545.